

# Entropy-vanishing Transition and Dynamical Heterogeneities in the Compressible Triangular Lattice Antiferromagnet

Hui Yin and Bulbul Chakraborty

*Martin Fisher School of Physics, Brandeis University, Waltham, MA 02454.*

(December 2, 2024)

## Abstract

In an effort to understand the glass transition, the kinetics of a spin model with frustration but no quenched randomness has been analyzed. The phenomenology of the spin model is similar to that of a supercooled liquid undergoing the glass transition. The slow dynamics exhibited by the spins can be associated with the presence of extended string-like structures which demarcate regions of fast spins. A thermodynamic phase transition, with the string density as the order parameter, can be related to the observed glass transition in the spin model.

## I. INTRODUCTION

The glass transition in supercooled liquids is heralded by anomalously slow relaxations with a time-scale diverging as the liquid freezes into the glassy state [1]. In recent years, there have been careful experimental and theoretical studies aimed at understanding the structural aspects of this transition. The presence and nature of dynamical heterogeneities near the glass transition has been a dominant underlying theme of both simulations [2,3] and experiments [4,5]. Simulations in Lennard-Jones liquids [2] have shown the existence of string-like dynamical heterogeneities and similar structures have been observed directly in colloidal glasses [5]. In the Adam-Gibbs scenario, the glass transition is related to a

phase transition accompanied by the vanishing of configurational entropy [6,7]. An explicit connection between (a) structural inhomogeneities, (b) anomalous relaxations and (c) the Adam-Gibbs scenario, even within the context of a simple model, would provide useful insight into the nature of the glass transition. In this work, we present our analysis of a simple model where there are naturally occurring dynamical heterogeneities in the form of strings and where there is an entropy vanishing transition involving these structures. Monte Carlo simulations of the model show that there is a glass-like transition with diverging time scales and an anomalously broad relaxation spectrum. We argue that the presence of the entropy-vanishing transition involving the string-like structures underlies this dynamical behavior.

The triangular-lattice Ising antiferromagnet (TIAFM) has an exponentially large number of ground states and has a zero-temperature critical point [8]. A mapping of the ground-states to dimer coverings reveals that these states can be characterized by string configurations which are the difference between dimer configurations [9,10]. Under periodic boundary conditions, the strings have to wrap around the system and they can only end at defects which are thermally activated [9,11]. Ground-states can, therefore, be classified according to string sectors. The number of states belonging to a particular string-density sector has been calculated [9] and, consistent with previously existing analysis of the TIAFM [12,13], the 2/3 string-density sector has been shown to have the largest entropy [9]. This reflects the fact that the 2/3 string density sector accommodates the largest number of free spins; spins with the most frustrated coordination where there are three satisfied bonds and three unsatisfied bonds. These spins are localized near the strings.

The effect of degeneracy-lifting fields on the TIAFM and the possibility of phase transitions has been studied extensively [11,13,14]. It has been shown that the nature of the phase transitions depends on whether thermal defects are allowed or not. In the zero-defect space, a staggered field [9] or anisotropic couplings [14] lead to a transition at which the string density and the entropy go to zero.

The model that we study is the *compressible* TIAFM (CTIAFM). Here the coupling

to the strain fields removes the exponential degeneracy of the ground-state and leads to a finite-temperature phase transition which is first-order [15,16]. It has been argued that the first-order transition circumvents an instability of the lattice towards a shear distortion [15]. We analyze the counterparts of these phase transitions in the zero-defect sector and show that the competition between energy gained from the lattice distortions and the extensive entropy of the TIAFM ground-states leads to a transition where the entropy vanishes. The transition is second order from the perspective of free-energy derivatives but has a discontinuous order parameter, the string density. This is reminiscent of the phase transitions in discontinuous spin glasses [19–21]. We have studied the dynamics of the supercooled phase, in the presence of thermally activated defects, using Monte Carlo simulations. These simulations indicate a glass-transition of the supercooled phase which we then analyze in the perspective of the phase transitions occurring in the zero-defect sector.

## II. COMPRESSIBLE TIAFM AND THE STRING PICTURE

The CTIAFM was originally introduced to study the role of elastic strain field in removing frustration [15]. The phase transitions of this model were subsequently reanalyzed in the context of effects of elastic strain fields on ordering transitions in alloys [16]. It was realized later that the supercooled phase of this model exhibits slow dynamics and at a certain quench temperature seems to fall out of equilibrium [17,18]. The nature of this ‘transition’ is the subject of this paper, and since we are interested in understanding the dynamics in terms of the string picture of the TIAFM ground-state, that is the perspective in which we present the model.

The Hamiltonian of the CTIAFM is given by:

$$H = J \sum_{\langle ij \rangle} S_i S_j - \epsilon J \sum_{\alpha} e_{\alpha} \sum_{\langle ij \rangle_{\alpha}} S_i S_j + N \frac{E}{2} \sum_{\alpha} e_{\alpha}^2 . \quad (1)$$

Here  $J$ , the strength of the anti-ferromagnetic coupling, is modulated by the presence of the second term which defines a coupling between the spins and the strain fields

$e_\alpha, \alpha = 1, 2, 3$ . The strain is homogeneous and is defined by the components along the three nearest neighbor directions on the triangular lattice. The parameter  $\epsilon$  determines the strength of the coupling. The last term stabilizes the unstrained lattice. The  $\epsilon$  term effectively introduces an anisotropy in the anti-ferromagnetic couplings, however, unlike the previously studied anisotropic TIAFM models [14], the anisotropy in the CTIAFM model is determined self-consistently by the strain fields. The exponential degeneracy of the TIAFM ground-states is lifted by the coupling to the strains and the ground-state of the CTIAFM is a three-fold degenerate striped phase where up down spins alternate between rows and there is a shear distortion characterized by  $e_1 = e$  and  $e_2 = e_3 = -e$  if the rows are along direction one [15].

Previous studies have shown that there is a finite-temperature transition between the paramagnetic and the striped phase and that this transition is first order [15,16]. In the next section we will analyze the counterpart of this transition in the limit of  $J \rightarrow \infty$  with  $\epsilon^2 J^2/E$  remaining finite, a transition that takes place within the manifold of the TIAFM ground-states.

The ground-states of the TIAFM are all those spin configurations which correspond to every triangle on the lattice having one and only one bond that does not satisfy the energy (*ie*, one ferromagnetic bond). The frustration in the model makes it impossible to have all bonds satisfied and, therefore, these configurations correspond to the lowest energy. All of these spin states can be mapped onto dimer coverings on the dual lattice [9,10]. The dimers are placed on the unsatisfied bonds and connect the centers of the triangles sharing this bond. Figure (1) shows such a dimer covering. Since every triangle has one unsatisfied bond, there is only one dimer ending at any point on the dual lattice. A useful classification of all the TIAFM ground-states is obtained by superposing a dimer configuration on a “standard” dimer configuration where all the dimers are vertical [9,10]. The number of strings measures the overlap of one of the many ground-states with a selected, standard ground-state configuration and the ground-states can be divided into different sectors according to this overlap [9].

The “striped” phase which is the ground-state of the CTIAFM has zero strings. It has been shown [9] that every sector with non-zero string density has an exponentially large number of states and therefore a finite entropy. The finite-temperature transition to the striped phase, therefore, has to be accompanied by a large change in entropy, and as we show in the next section, the transition within the ground-state manifold is an entropy-vanishing transition. In the limit of  $J \rightarrow \infty$  (other parameters remaining finite), the CTIAFM energy function can be written in terms of the string density. The crucial difference of this energy function from the anisotropic TIAFM [14] or the TIAFM in the presence of a staggered field [9] is that this energy function is quadratic in the string density. This is a consequence of the anisotropy being determined self-consistently. A useful analogy is to think of the anisotropy as a quenched variable in the earlier model [14] but as an annealed variable in the CTIAFM. Recent studies of thermodynamics of glasses [7,22] have introduced a coupling between different replicas and the CTIAFM is reminiscent of the annealed version of this model [22].

The strings are also relevant from a dynamical standpoint. Considering purely local dynamics (spin-flip, spin exchange etc), the system is confined to relax within the string sector determined by the initial string density: the dynamics is strongly non-ergodic. Relaxations within a string sector depend on the string density of the sector since the dynamics of spins near the strings is very different from the dynamics of spins far away from the strings. Assuming spin-flip dynamics for the moment, the only spins that can be changed while the system remains in the ground-state manifold, are the ones which have a coordination of 3-3 (3 satisfied and 3 unsatisfied bonds). These are the most frustrated spins in the system and they are located at isolated kinks on the strings, as shown in Figure (2). For a high string-density configuration, these spins are distributed essentially homogeneously through the system since the strings are closely spaced. In configurations with few strings, the distribution of fast spins is extremely inhomogeneous (Fig 3) and the fast spins are organized in linear structures along the strings. Relaxations in these low-density sectors involve local fluctuations occurring over short times which are not very effective at de-correlating the

spins and large-scale motion of the strings which homogenizes the system and is effective at de-correlating the spins. These large scale motions occur over very long time scales. We will present Monte Carlo results of spin-spin autocorrelation functions which agree with this qualitative assessment.

The string picture is strictly valid at  $J = \infty$ . At finite  $J$ , defects occur which correspond to triangles with all three bonds unsatisfied. These defects can terminate the strings [11] and at very high temperatures the string picture breaks down.

### III. PHASE TRANSITIONS IN THE ZERO-DEFECT SECTOR

The spin states in the absence of defects ( $J \rightarrow \infty$ ) can all be classified according to the number of strings, or equivalently the string density  $p = N_s/L$  where  $L$  is the linear dimension of the sample and  $N_s$  is the number of strings. In the absence of any degeneracy-lifting couplings, all of these states have the same energy. The number of spin states ( $\Omega(p)$ ) belonging to a particular string-density sector  $p$  has been calculated and this number has been shown to be exponentially large [9]:

$$\Omega(p) = \exp(N\gamma(p)) ,$$

where  $N = L \times L$  is the total number of spins. The entropy  $\gamma(p)$  has a peak at  $p = 2/3$  [9]. A plot of the function  $\gamma(p)$  is shown in Fig. (4). Since the energy is independent of the string density, at any finite temperature, the  $p=2/3$  states dominate the configurations of the TIAFM.

In the compressible model, the energy depends on the string density. From the Hamiltonian of the CTIAFM (Eq. 1), it can be seen that the strain field, along a particular direction,  $\alpha$ , couples to the average  $\langle S_i S_j \rangle_\alpha$ . In the absence of defects, this average counts the number of strings along the  $\alpha$  direction, *i.e* the number of strings obtained by taking an overlap with the standard dimer state with all the dimers perpendicular to the  $\alpha$  direction. Any two states related by flipping all the spins have the same energy, however, the energy is now determined by the set  $p_\alpha, \alpha = 1, 2, 3$ , the string densities along the three directions:

$$E = H/N = \epsilon J \sum_{\alpha} e_{\alpha} (1 - 2p_{\alpha}) + \frac{E}{2} \sum_{\alpha} e_{\alpha}^2 \quad (2)$$

where we have left out an infinite constant. The strain field appears in the Hamiltonian as a purely Gaussian variable and can be integrated out to yield an energy function depending only on the string densities:

$$E(\{p_{\alpha}\}) = -(\mu/2) \sum_{\alpha} (1 - 2p_{\alpha})^2 \quad (3)$$

Here  $\mu = \epsilon^2 J^2 / E$  is the relevant coupling constant which stays finite as  $J \rightarrow \infty$ . The constraint of no defect translates into a constraint on the string densities and it can be easily shown that  $p_1 + p_2 + p_3 = 2$ . This simply expresses the constraint that there is only one unsatisfied (ferromagnetic) bond per triangle. Only two of the three string densities are, therefore, independent. Periodic boundary conditions, which force the strings to wrap around, restrict the configurations to only those where at least two of the string densities have to be equal. The energy of these states can be written in terms of one string density,  $p_1 = p$ , for example with  $p_2 = p_3 = 1 - p/2$ ;

$$E(p) = -(\mu/2)((1 - 2p)^2 + 2(1 - p)^2) . \quad (4)$$

The partition function, in the zero defect sector, is expressed in terms of this energy and the entropy  $\gamma(p)$  as

$$Z = e^{-\beta F} = \sum_p e^{-\beta NE(p) + N\gamma(p)} \quad (5)$$

where  $N$  is the total number of spins in the system and  $\beta$  is the inverse temperature. In the thermodynamic limit, the partition function sum is dominated by the string density which minimizes the function  $f(p) = \beta E(p) - \gamma(p)$ . The partition function  $Z$  has the appearance of a mean-field model and this is a consequence of the homogeneous nature of the strain fields which induce a long-range four-spin interaction [16]. Fig (4(b)) shows the function  $f(p)$  at different values of  $\beta\mu$ . At high temperatures, the free-energy function has only one minimum at  $p = 2/3$ . As the temperature is lowered, this minimum stays pinned at  $2/3$

and a second minimum starts developing at  $p = 0$ . The  $p = 0$  state stays metastable until the temperature is lowered to  $T_1$  where the free energy of the  $p = 0$  state becomes equal to that of the  $p = 2/3$  state. This occurs at  $\beta\mu = (3/4) * \gamma(2/3) \simeq 0.24$  and there is a first-order transition from the  $p = 2/3$  state to the  $p = 0$  state. The  $p = 2/3$  state loses its metastability at a still lower temperature  $T^*$ . The transition at  $T_1$  is a standard first order transition with discontinuities in both the order parameter  $p$  and the derivatives of the free energy. In the mean-field limit, all metastable states have infinite lifetimes and the transition at  $T_1$  is invisible to the system when quenched from a high temperature where it has equilibrated into the  $p = 2/3$  state. The transition at  $T^*$  is very different. The order parameter shows a discontinuous change from  $p = 2/3$  to  $p = 0$ , however, the transition is second-order according to the Ehrenfest criterion and is reminiscent of the transitions observed in p-spin spin glasses [7]. The entropy also vanishes discontinuously at  $T^*$  and the low temperature phase is frozen into one of the ground-states with no excitations. The transition at  $T^*$  is similar to the ones observed in TIAFM with anisotropic couplings [11] and TIAFM in the presence of a staggered magnetic field [9], in being an entropy-vanishing transition, however the nature of the transition is different.

The value of  $T_1$  for  $\mu = 0.18$  is 0.74 (*cf* Fig. (4(b)) which is comparable to the first-order transition temperature of 0.67 observed at finite  $J$  for the same value of  $\mu$  [15,16]. The finite- $J$  transition line does not follow the line  $\beta\mu = 0.24$  [15,16] but approaches this line asymptotically as  $J \rightarrow \infty$ .

Purely relaxational dynamics, where the string density is allowed to relax in a free-energy surface with its topology evolving as a function of temperature, as shown in Fig. (4b), would lead to critical slowing down, with the string-density relaxation time diverging as  $T^*$  is approached. Below  $T^*$ , one could expect to see some interesting dynamics because of the “flatness” of the free-energy surface near  $p = 2/3$ . The more interesting question to ask is what the nature of the dynamics is when the kinematics is spin flip (or spin exchange) rather than string density updates. In the space of zero-defect states, any local dynamics is strongly non-ergodic since the system can explore only a fixed string-density sector. At

finite  $J$ , defects appear and there are thermally activated processes leading to transitions from one string sector to another. In the next section, we present results of our Monte Carlo simulations using spin-exchange kinetics and analyze them in the light of the phase transition at  $T^*$ .

#### IV. DYNAMICS OF THE SUPERCOOLED STATE FOR FINITE $J$

The nature of the supercooled state of the CTIAFM at finite  $J$  was analyzed using Monte Carlo simulations. The system was instantaneously quenched from a temperature well above the known first-order transition temperature [16] to temperatures below this temperature. The value of the parameter  $\mu$ , used in these simulations, was 0.18 which corresponds to a region of strong first-order phase transitions [16], and  $J$  was taken to be 1. Spin-exchange kinetics was extended to include moves which attempted changes of the strain fields  $e_\alpha$ . Details of the simulation algorithm have been published earlier [16]. System sizes ranged from 48x48 up to 120x120. Unless otherwise stated, the results presented in this section were obtained from 96x96 systems. The simulations were always started from a state in the  $p = 2/3$  sector.

The behavior of the spin-spin autocorrelation function,  $C(t) = (1/N)\sum_i S_i(t + t_0)S_i(t_0)$ , is shown in Fig. (5). The spin relaxation is seen to be non-exponential. The functional form that best fits the data is a power law with an exponential cutoff. These fits are shown in Fig. (5). The power-law exponent, obtained from the fits, has a value of  $\simeq 0.33$  for temperatures higher than 0.47. The time scale associated with the exponential cutoff shows a strong temperature dependence akin to the Vogel-Fulcher form [23] and appears to diverge around  $T = 0.47$ . We will discuss this time scale further in the context of string relaxations. The power-law exponent at  $T = 0.47$  is smaller than 0.33 and upon closer analysis, it was found that for  $T \leq 0.47$ , the autocorrelation function  $C(t)$  depends on the *waiting time*. Fig (6) shows the energy autocorrelation function  $C_E(t)$  obtained from averaging over different ranges of  $t_0$ , the time origin chosen in the calculation of  $C_E(t)$ . The

energy autocorrelation function carries information similar to  $C(t)$  but its calculation is less computationally intensive. These results show that  $C_E(t)$  does not depend on the time origin for  $T > 0.47$  but begins to do so below this temperature. This transition is reminiscent of the glass transition in a supercooled liquid.

In view of the string picture of the spin states, presented in the last section, it is natural to ask whether the strings show any interesting behavior as the transition at  $T = 0.47$  is approached. The string-density autocorrelation function, measured in the simulations, are well described by exponential relaxations, in contrast to the spin-spin autocorrelation functions. The string-relaxation time scale, obtained from the exponential fits, are plotted as a function of temperature in Fig. (7). As seen from the figure, this time scale appears to diverge and the divergence is of the Vogel-Fulcher type; much stronger than rather power-law divergences associated with critical points. The time scales appearing in Fig. (7) are extremely long and hints at the difficulties of making equilibrium measurements at these temperatures. As mentioned earlier, the time scale associated with the exponential cutoff of  $C(t)$  also appears to diverge, and we find that this time scale is similar to and has the same temperature dependence as the string relaxation time.

In order to investigate the nature of the string-relaxations further, we measured the distribution,  $P(\Delta p)$ , of  $\Delta p = p(t + t_0) - p(t)$ , the deviation of the string density in time  $t$ . The distributions were generated by choosing different time origins  $t_0$ . The most striking feature of the distributions, observed at temperatures close to  $T = 0.47$ , is its non-Gaussian nature at intermediate times. At  $T = 0.55$ , the non-Gaussianity is most pronounced at  $t = 4000$ . Beyond this time the distribution relaxes to a Gaussian and beyond  $t = 8000$ , the distribution is time independent and no significant non-Gaussian character is observed. At  $T = 0.47$ , a time-independent behavior is not observed for times as long as 30,000 and the distributions are non-Gaussian at all intermediate times. At very high temperatures, the times needed to reach a stationary distribution are short and the distributions are Gaussian. Based on the dynamics of systems near critical points [24], one would expect to find a distribution of  $\Delta p$  which takes longer to reach its time-independent form as the critical

point is approached and to find non-Gaussianity (within the limits of finite-size cutoffs) in the stationary distribution. In contrast, the current systems exhibits non-Gaussianity at intermediate times. This scenario is intriguing and suggests that there is a time-dependent length scale in the system which diverges as  $T \rightarrow 0.47$ , *i.e.*,  $\xi(\tau, T) \rightarrow \infty$  as  $T \rightarrow 0.47$ , and  $\tau$  itself diverges as this transition is approached [25]. The thermodynamic transition present in the zero-defect sector seems to have been replaced by a dynamical transition at a temperature close to  $T^* \simeq 0.4$  (for  $\mu = 0.18$ ). One would expect the zero-defect scenario to be valid as long as there are few events that take the system out of this sector. Since these events are correlated with the appearance of thermally activated defects, it seems feasible that there is a time-scale beyond which the zero-defect analysis breaks down, and that this time scale increases with decreasing temperature. The Vogel-Fulcher-like behavior of the string relaxation time is likely to be a consequence of the interplay between an intrinsically diverging time scale and the fact that the strings can relax only via the thermally activated defects.

Based on our association of the dynamical transition with the real thermodynamic transition, we would expect the temperature of the dynamical transition to track  $T^*$  as the effective coupling constant  $\mu$  is varied. We have not performed detailed simulations at values of  $\mu$  other than  $\mu = 0.18$ , however, preliminary results at  $\mu = 6$  where  $T^* \simeq 13$  indicate a dynamical transition around  $T = 10$ .

A picture of the spin relaxation can be pieced together from these observations. The spins undergo power-law relaxation within a given string sector and this power law is interrupted by the system making a transition to a different string sector. The time scale for this latter process is given by the string-density relaxation time. The divergence of time scales is, in this picture, completely dictated by the dynamics of the strings. In our Monte Carlo simulations, the initial state was always chosen to be in the  $p = 2/3$  sector and this could be the reason for the temperature-independent power law observed in Fig. (5). The dynamics of the spins is essentially an average of the dynamics in different string sectors weighted by the probability of sampling a given string sector. If the distribution of string densities is narrow

and centered around  $2/3$ , then the homogeneous dynamics of this sector will dominate. If the distribution is broad, however, the spin dynamics will reflect the intrinsic dynamics of the different sectors. In order to investigate the spin relaxation in a *given* string-density sector, we have performed Monte Carlo simulations keeping the string-density fixed. These results are shown in Fig. (9). The nature of the relaxations is different in the different string sectors. For  $p \geq 1/4$ , the relaxation is well described by a power-law with an exponent  $\simeq 1/3$ . The observed value of  $0.33$  in the  $C(t)$  plots shown in Fig. (5) is consistent with this and indicates that the  $2/3$  sector dominates the dynamics when we start from this initial state. At string densities lower than  $1/4$ , the relaxation is better described by a stretched exponential with a stretching exponent  $\simeq 1/3$ . As mentioned earlier, the relaxation in these string sectors is expected to be inhomogeneous as there are regions of fast and slow spins, and this is consistent with the observation of a stretched exponential behavior. With random initial conditions, where the system is started from different string sectors, the spin-relaxation should reflect the intrinsic dynamics of the low string-density sectors and the relaxation spectrum is expected to exhibit a temperature-dependent shape [26].

## V. CONCLUSIONS

Our study of the CTIAFM provides strong indication that the slow, “glassy” dynamics in this model is associated with an entropy-vanishing transition involving extended, string-like structures. These structures are a manifestation of the frustration embodied in the nearest-neighbor, anti-ferromagnetic interactions, and the entropy-vanishing transition is a consequence of coupling to another degree of freedom, the lattice strain, which tends to remove the frustration in the system. The strings are naturally occurring dynamical heterogeneities: they demarcate regions of fast spins. In a lattice model, such as the CTIAFM, the frustration leads to these well-defined geometrical structures. The anomalously slow dynamics owes its origin to these extended structures. The time scale for string relaxations suffers critical slowing down because of the underlying phase transition. The effect is, however, en-

hanced since transitions from one string sector to another can only take place via activated dynamics involving the defects. It is also interesting to note that the spin dynamics within a string sector depends on the string density.

It is tempting to speculate that the clusters of mobile particles observed in Lennard-Jones simulations [2] and in colloidal systems [5] comprise of the most frustrated particles in the system. In a Lennard-Jones mixture, these should be the particles with the least number of unlike bonds (if unlike bonds are energetically preferred) and in a colloidal system, these should be the particles which have coordinations that are furthest from being icosahedral. An experimental test of this correlation between geometry and mobility would lend credence to the idea that the glass-transition is a manifestation of an entropy-vanishing transition involving extended structures which are forced in by frustration.

The work of BC was supported in part by NSF grant number DMR-9815986 and the work of HY was supported by DOE grant DE-FG02-ER45495. We would like to thank R. K. P. Zia, W. Klein, H. Gould, S. R. Nagel and J. Kondev for many helpful discussions.

## REFERENCES

- [1] C. A. Angell, *J. Phys. Chem.* **49**, 863 (1988), M. D. Ediger, C. A. Angell, and S. R. Nagel, *J. Phys. Chem.* **100**, 13200 (1996) W. Götze and L. Sjogren, *Rep. Prog. Phys. B* **55**, 241 (1992)
- [2] C. Donati, J. F. Douglas, W. Kob, S. J. Plimpton, P. H. Poole and S. C. Glotzer, *Phys. Rev. Lett.* **80**, 2338 (1998); W. Kob, C. Donati, S. J. Plimpton, P. H. Poole, and S. C. Glotzer, *Phys. Rev. Lett.* **79**, 2827 (1997); C. Donati, S. C. Glotzer, P. H. Poole, W. Kob, and S. J. Plimpton, *Phys. Rev. E* **60**, 3107 (1999).
- [3] G. Johnson, A. Mel'cuk, H. Gould, W. Klein and R. Mountain, *Phys. Rev. E* **57**, 5707 (1998); W. Klein, H. Gould, J. Tobochnik, F. J. Alexander, M. Anghel and G. Johnson, preprint cond-mat/0001230.
- [4] M. T. Cicerone and M. D. Ediger, *J. Chem. Phys.* **103**, 5684 (1995) and references therein.
- [5] E. R. Weeks, J. C. Crocker, A. C. Levitt, A. Schofield, D. A. Weitz, *Science* **287**, 627 (2000); W. K. Kegel, A. van Blaaderen, *Science* **287**, 290 (2000).
- [6] G. Adam and J. H. Gibbs, *J. Chem. Phys.* **43**, 139 (1965), J. H. Gibbs and E. A. DiMarzio, *J. Chem. Phys.* **28**, 373 (1958).
- [7] M. Mezard and G. Parisi, preprint cond-mat/0002128, and references therein.
- [8] C. Zeng and C. L. Henley, *Phys. Rev. B* **55**, 14935 (1997)
- [9] A. Dhar, P. Choudhuri and C. Dasgupta, *Phys. Rev. B* **61**, 6227 (2000).
- [10] C. Zeng, P. L. Leath and T. Hwa, *Phys. Rev. Lett.* **83**, 4860 (1999).
- [11] Henk W. J. Blöte and M. Peter Nightingale, *Phys. Rev. B* **47**, 15046 (1993) and references therein.
- [12] G. H. Wannier, *Phys. Rev.* **79**, 357 (1950).

- [13] R. M. F. Houtappel, *Physica* **16**, 425 (1950)
- [14] H. W. J. Blöte, H. J. Hilhorst, *J. Phys. A: Math. Gen.* **15**, L631 (1982).
- [15] Z. Y. Chen and M. Kardar, *J. Phys. C* **19**, 6825 (1986).
- [16] Lei Gu, Bulbul Chakraborty, P. L. Garrido, Mohan Phani and J. L. Lebowitz, *Phys. Rev. B* **53**, 11985 (1996).
- [17] Lei Gu and Bulbul Chakraborty, *Mat. Res. Soc. Symp. Proc.* **455**, 229 (1997), and cond-mat/9612103; Lei Gu, Ph. D. Thesis, Brandeis University, 1999.
- [18] B. Chakraborty, L. Gu and H. Yin, preprint cond-mat/0003306, to appear in *J. Phys. Condens. Mat.*, 2000.
- [19] D. J. Gross and M. Mezard, *Nucl. Phys.* **B240**, 431 (1984)
- [20] T. R. Kirkpatrick and P. G. Wolynes, *Phys. Rev. A* **34**, 1045 (1986), *Phys. Rev. A* **35**, 3072 (1987), T. R. Kirkpatrick and D. Thirumalai, *Phys. Rev. Lett.* **58**, 2091 (1987), *Phys. Rev. B* **36**, 5388 (1987),
- [21] J. P. Bouchaud and M. Mezard, *J. Phys. I* **4**, 1109 (1994).
- [22] S. Franz and G. Parisi, *Phys. Rev. Lett.* **79**, 2486 (1997) and *Physica A* **261**, 317 (1998).
- [23] H. Vogel, *Phys. Z.* **22**, 645 (1921), G. S. Fulcher, *J. Am. Ceram. Soc.* **8**, 339 (1925)
- [24] N. Goldenfeld, *Lectures on Phase Transitions and the Renormalization Group*, (Addison-Wesley, New York, 1992).
- [25] G. Parisi, preprint cond-mat/9801034; S. Franz, C. Donati, G. Parisi and S. C. Glotzer, *Phil. Mag. B* **79**, 1827 (1999)
- [26] P. K. Dixon *et al*, *Phys. Rev. Lett.* **65**, 1108 (1990); N. Menon and S. R. Nagel, *Phys. Rev. Lett.* **74**, 1230 (1995).

## FIGURES

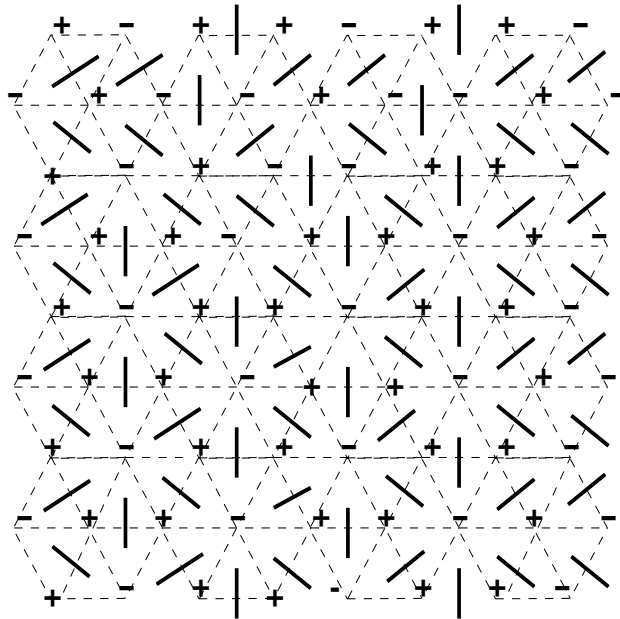


FIG. 1. Mapping of one of the TIAFM ground-states to a dimer covering on the dual lattice.

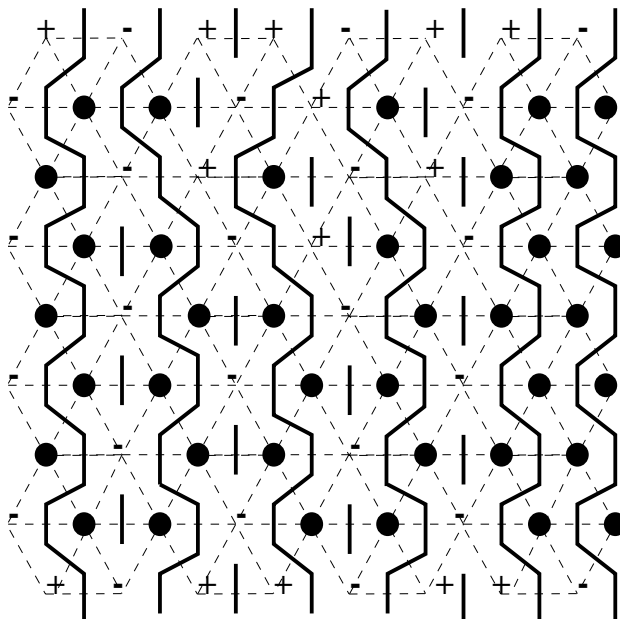


FIG. 2. String configuration with a string density  $\simeq 2/3$ . The fast spins, the ones with 3 – 3 coordination, are marked by shaded circles and are seen to be homogeneously distributed.

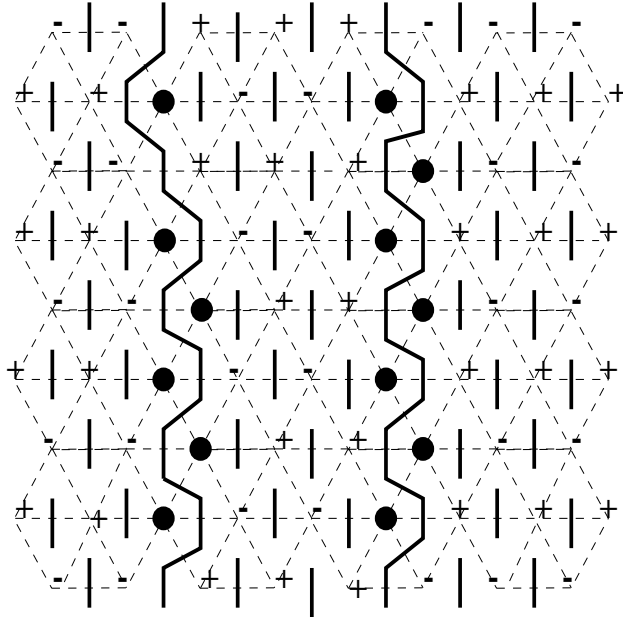


FIG. 3. String configuration with string density close to zero. The fast spins are shown by shaded circles and now form string-like clusters.

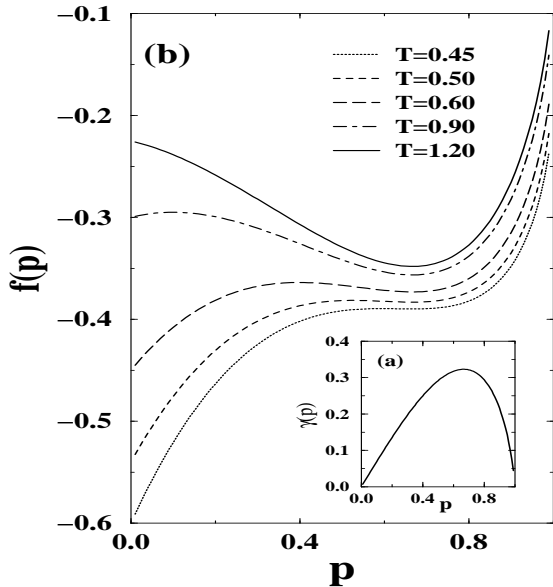


FIG. 4. (a) Entropy as a function of the string density from the work of Dhar et al. ([9])  
 (b) The dimensionless free energy,  $f(p)$ , in the zero-defect limit, as a function of string density at different temperatures for  $\mu = 0.18$ , the value used in the Monte Carlo simulations. Temperature is measured in units of  $1/k_B$ .

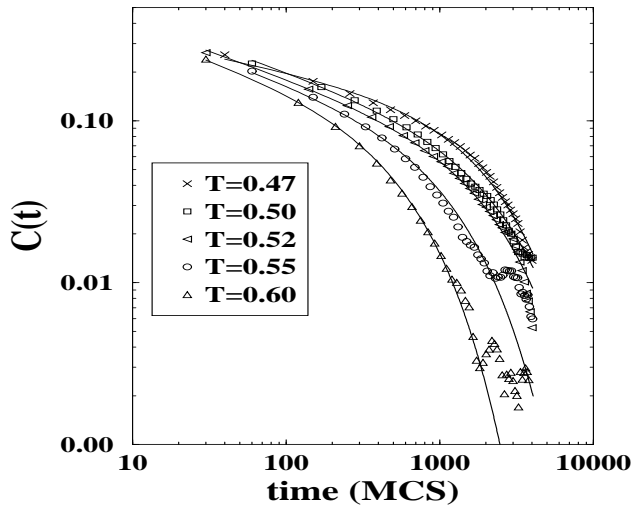


FIG. 5. Spin-Spin autocorrelation function at temperatures approaching  $T = 0.47$  (measured in units of  $1/k_B$ ). The fits, shown as solid lines, are to power laws with an exponential cutoff. The power-law exponent is  $\simeq 0.33$  for all temperatures higher than 0.47. The time-scale of the exponential cutoff is proportional to the string-density relaxation function (*cf. text*).

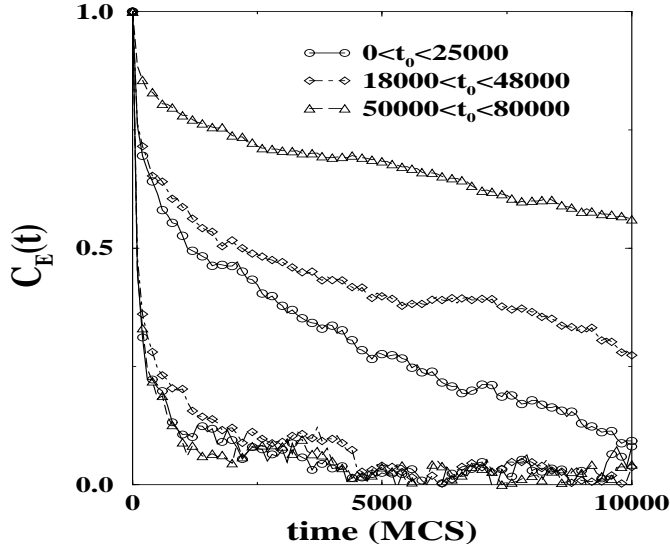


FIG. 6. Waiting-time dependence of the energy autocorrelation function. The lower set of curves are from quenches to  $T = 0.55$  and the upper set from quenches to  $T = 0.47$

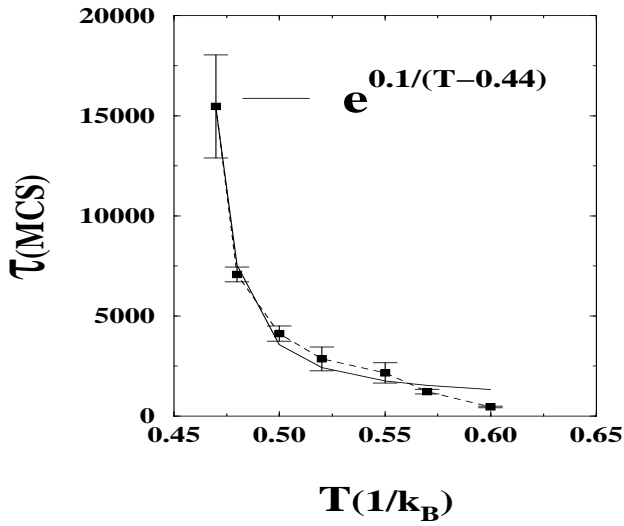


FIG. 7. Temperature dependence of the string-density relaxation time. The fit is to a Vogel-Fulcher form.

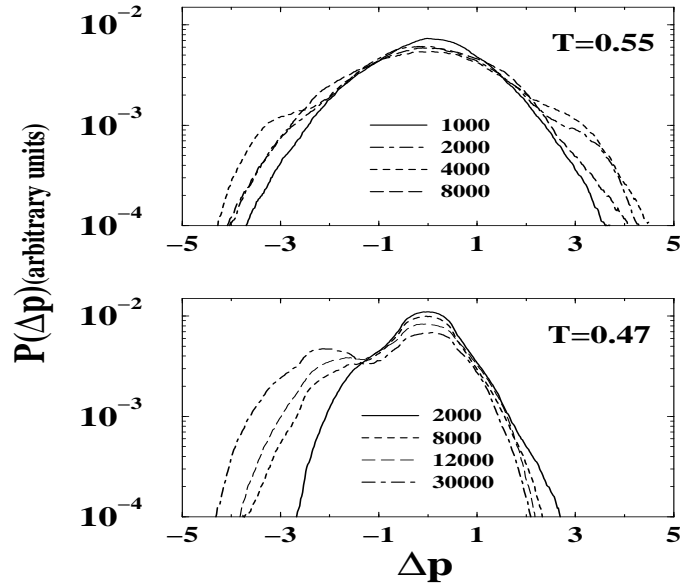


FIG. 8. Distribution of string-density deviation  $\Delta p(t)$ , at  $T = 0.55$  and  $T = 0.47$ , showing non-Gaussian behavior at intermediate times. The area under the curves have been normalized to unity.

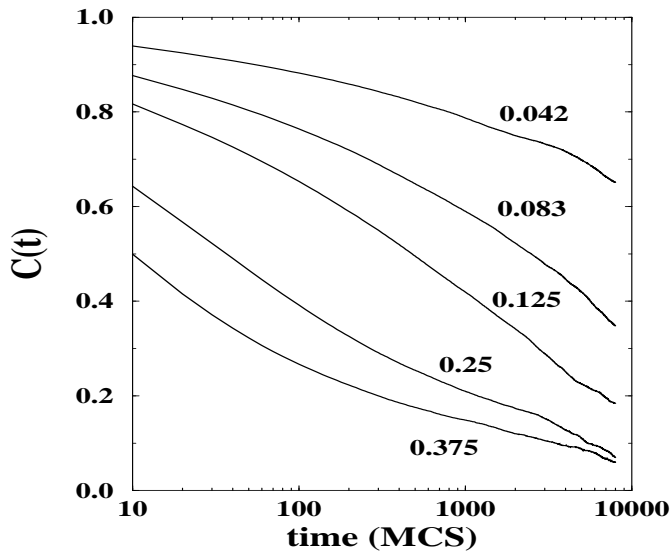


FIG. 9. Spin-spin autocorrelation function in different string-density sectors. The curves are labeled by the value of the string density,  $p$ .